3. Overview and construction status of the RIBF accelerators

3.1 Introduction

The RIBF accelerators, the fRC, the IRC and the SRC, are being constructed on schedule for completion in the summer of 2006. The first beam is scheduled by the December of 2006. The schedule of the construction of these accelerators including the beam lines between them is shown in Fig. 3.1.1.

R&D on the production of U ion beams, the additional installation of a flattop resonator in the RRC, and so on are also being carried out.

In this report are described overview and construction status of the accelerators as well as the R&D's work. For further details, refer to the corresponding reports in the attached document "Collected papers on the accelerators for the RIKEN RI beam factory (2003-2005)".

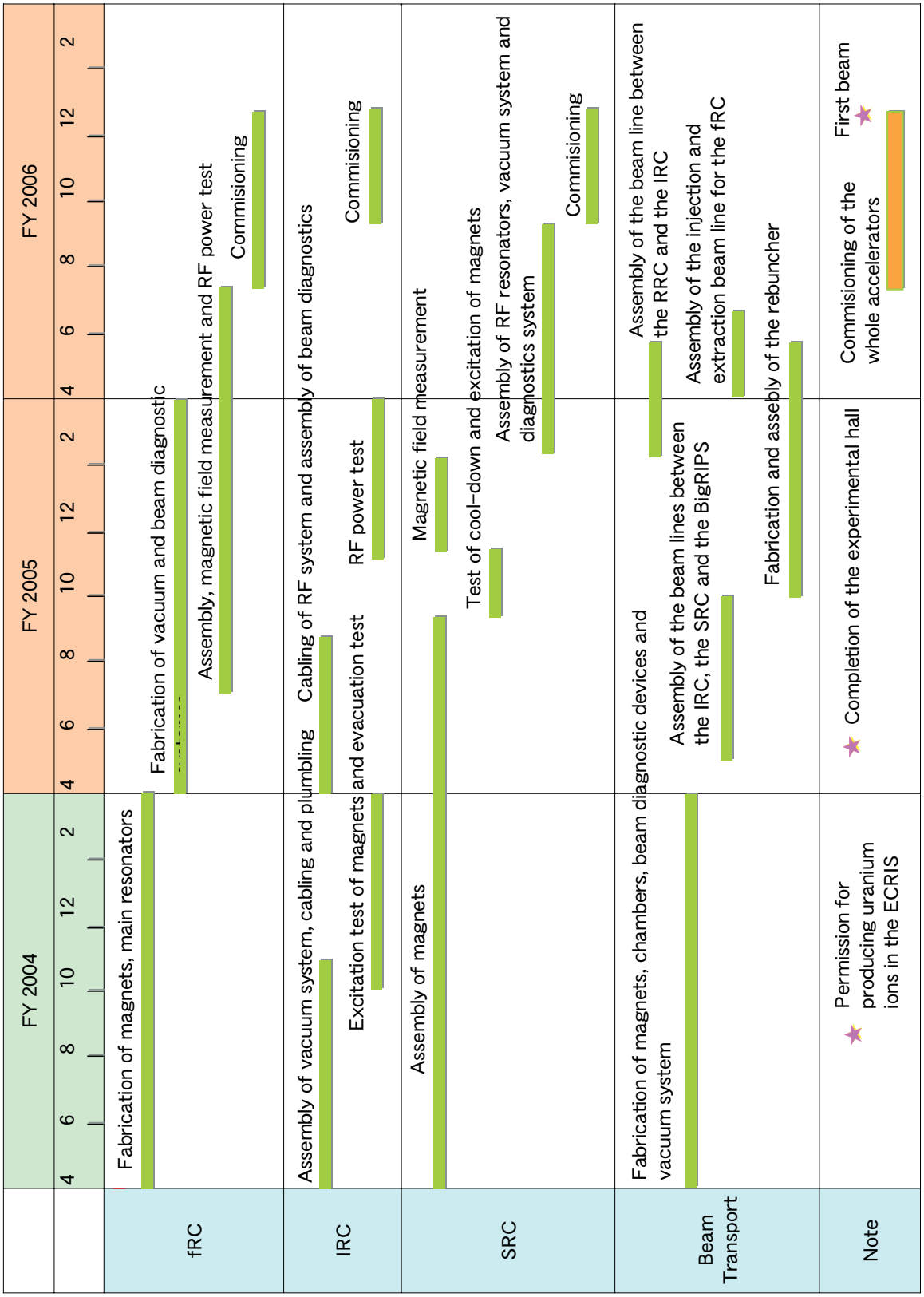

Figure 3.1.1. Construction schedule for the RIBF accelerators.

3.2 fRC

Outline

The fRC is a room-temperature, fixed-frequency ring cyclotron with K-570 MeV and located between the RRC and the IRC. The fRC is installe in the E4 experimental room of the RARF building. Main parameters of the fRC are listed in Table 3.2.1. Layout of the fRC in the E4 experimental room and a plan view of view of the fRC are shown in Fig. 3.2.1 and Fig. 3.2.2, respectively. The fRC consists of four sector magnets, beam injection and extraction elements, two acceleration and one flattop rf resonators, and some kinds of beam diagnostic instruments. The average radii of the injection and the extraction are 1.55 m and 3.30 m, respectively, which were determined by taking account of energy losses through two charge strippers placed upstream and downstream of the fRC. In the case of uranium ions, energy losses by the upstream and downstream charge strippers are considered to be 0.4 and 4.5 MeV/nucleon, respectively. The injection and extraction energies are accordingly reduced/increased to be 10 MeV/nucleon and 51 MeV/nucleon, respectively. For lighter ions the injection radius is adjusted so as to match respective injection energies. Acceleration rf frequency is 55.0 MHz. The maximum magnetic rigidity of the extraction beam is 3.57 Tm.

Sector magnets

The sector magnets of the fRC were designed based on those of the RRC and the IRC. Fundamental structure of the poles and yokes is a stack of low carbon steel plates with a thickness of 290 mm at the maximum. Since the fRC is installed in the E4 experimental room, where the height of beam line above the floor level is as short as 1.7 m, special care had to be taken on the design of height of the sector magnets in order to match this condition. The height of the sector magnet thus must be less than 3.4 m. This height is about 65 % of the height of the RRC, which is almost the same size as the fRC in terms of the K-value (540 MeV for the RRC). Despite that the fRC is operated at the fixed frequency, i.e. a fixed energy cyclotron, charge-to-mass ratios and then the isochronous field distributions are different for different kinds of ions. Therefore, the profile of the pole edge was designed so as to minimize these differences.

Table 3.2.2 shows the main parameters of the sector magnets. The pole gap, sector angle, height and total weight are 50 mm, 58 deg, 3.34 m and 1480 t, respectively. The maximum magnetic field is 1.68 T with the maximum main coil current of 650 A. The total power consumption of the main coil is 60 kW/sector. The sector magnet of the fRC will be equipped with 10 pairs of trim coils. The maximum currents are 200 A for six pairs and 100 A for the other four pairs. The total trim coil current for one sector is 3 kA, which is much less than that

of the IRC of 18 kA. By the reduction of the current, the structure of the trim coil could be simplified; the trim coil was designed to be a coaxial double tubes consisting of a copper pipe inserted in a stainless pipe with insulation glass tapes in between. Therefore, they could be exposed directly to the high vacuum of the beam chamber as shown in Fig. 3.2.3, while the trim coils for the RRC and the IRC are in a sub-vacuum chamber. Adopting this structure, the pole gap of the fRC could be shortened to 50 mm compared with the gap of 80 mm of the RRC and the IRC. The upper and lower poles thus form a vacuum chamber and so the surface of the pole is coated with Ni to avoid outgas from iron.

The magnetic field distributions along the sector-center line as well as the magnet edge region were measured at the factory. The whole sector magnets have been installed and assembled at the due place in the E4 experimental room; a photograph of the sector magnets is shown in Fig. 3.2.4.

Injection and extraction system

The injection and extraction system is similar to that of the RRC and the IRC. The injection system consists of one electrostatic inflection channel (EIC), two magnetic inflection channels (MIC1 and MIC2), one bending magnet (BM1) and two quadrupole magnets. The extraction system consists of one electrostatic deflection channel (EDC), two magnetic deflection channels (MDC1 and MDC2) and two bending magnets (EBM1 and EBM2). Table 3.2.3 shows parameters of the injection and extraction devices.

Rf system

The yoke of the sector magnet was designed to be short and wide because of the limitation of the height coming from the E4 room condition, the space for the resonators were limited. Therefore, we chose the rf frequency to be three times that of the RILAC and the RRC in order to reduce the size of the resonators. The rf frequency of the main resonator is 55 MHz; that of the flattop resonator is 165 MHz. The adoption of this higher frequency reduces the phase acceptance of the fRC, but this reduction will be compensated with a rebuncher installed between the RRC and the fRC.

Two main resonators and one flattop resonator are used. The main resonator is of a single-gap type, which is similar to that of the IRC and SRC but without a tuning panel. The maximum voltage is expected to be about 500 kV with the consumption power of 100 kW that is fed by a final amplifier based on a tetrode (SIEMENS RS2042SK) with a grounded-grid circuit. The electrical characteristics of the resonators were measured at the factory. Figure 3.2.5 and 3.2.6 show photographs of the resonator sitting at the factory and being installed temporarily in the E4 room, respectively. A close-up view of the acceleration

gap of the responatoris shown in Fig. 3.2.7.

Vacuum system

The vacuum pumping equipment consists of 6 cryopumps with 13,000 L/sec used for the main evacuation, and two turbo-molecular pumps and two mechanical-booster pumps used for the rough evacuation. The pressure is expected to be $1x10^{-6}$ Pa.

Beam diagnostics

The beam diagnoatic system consists of one main differential probe (MDP), one extraction radial probe (ERP) and one set of phase probes (PP). The beam sensor part of IRP2 is of a block type, and those of the IRP1 and ERPs are of a wire type with three tungsten filaments. The phase probe is equipped with 14 pairs of electrodes.

Table 3.2.1. Main parameters of the fRC.

K-value	570 MeV
Number of sector magnets	4
Harmonics	12
Injection radius	1.55 m
Extraction radius	3.30 m
Velocity gain	2.12
Maximum energy	50.7 MeV/nucleon
Maximum magnetic rigidity	3.57 Tm
Number of rf resonators	
Main acceleration	2
Flattop	1
Rf frequency	
Main acceleration	55 MHz
Flattop	165 MHz

Table 3.2.2. Main parameters of the sector magnet.

Pole gap	50 mm
Sector angle	58 deg
Height	3.34 m
Total weight	1480 t
Maximum magnetic field	1.68 T
Main coil	
Maximum current	650 A
Maximum ampere-turns	91 kA/sector
Maximum power consumption	60 kW/sector
Trim coil	
Number of trim coils	10 pairs/sector
Maximum current	200 A
Maximum power consumption	5 kW/sector

Table 3.2.3. Parameters of the beam injection and extraction channels.

Magnetic devices			
Device	Bend angle (deg)	Radius (m)	B (T)
MIC1	40	0.87	0.16
MIC2	80	0.72	0.16
MDC1	19	2.15	-0.06
MDC2	20	2.30	-0.14
Electrostatic deflector			
Device	Length(m)	gap (mm)	E(kV/cm)
EIC	0.5	12	100
EDC	0.55	12	100

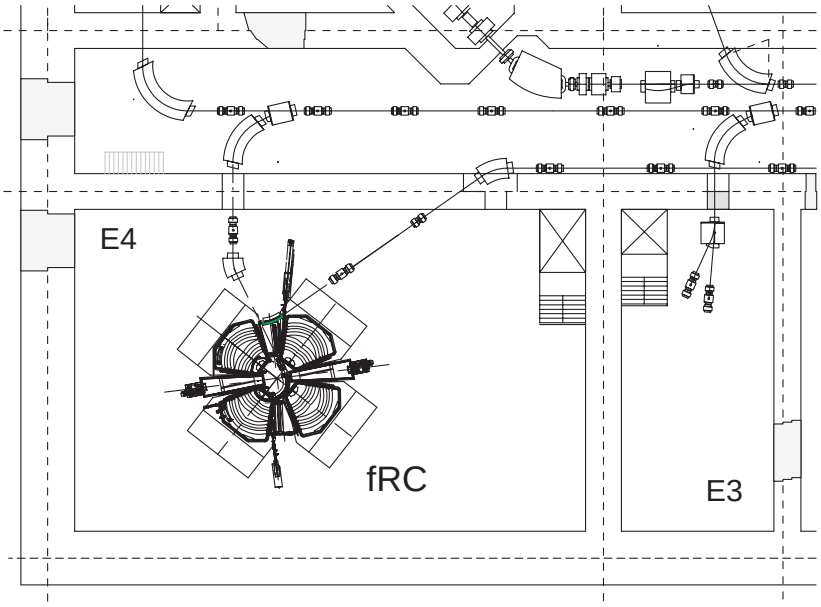

Figure 3.2.1. Layout of the fRC in the E4 experimental room.

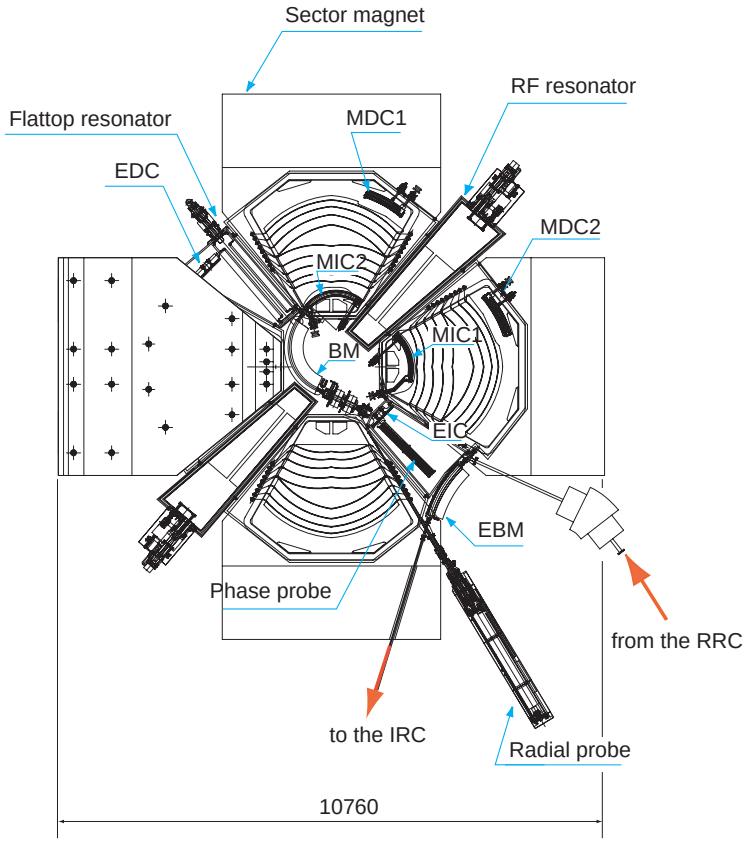

Figure 3.2.2. Plan view of the fRC.

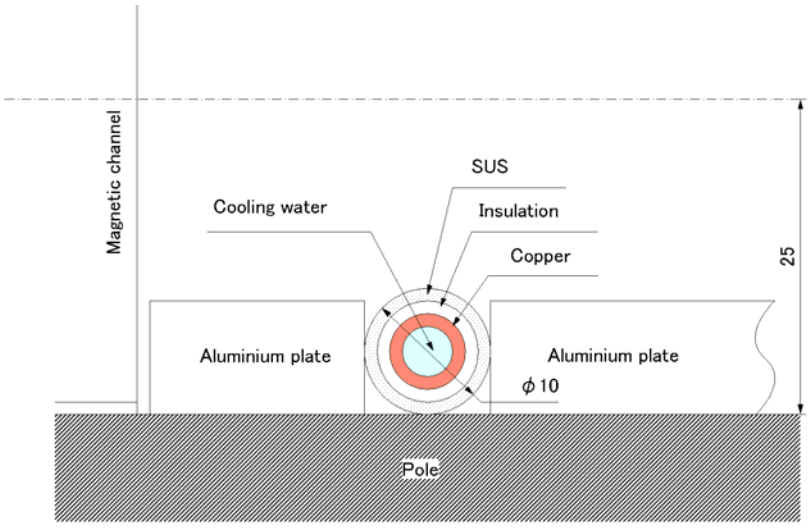

Figurer 3.2.3. Cross-section of the trim coil.

Figure 3.2.4. Sector magnets of the fRC in the E4 experimental room.

Figure 3.2.5. Photograph of the main resonator sitting at the factory.

Figure 3.2.6. Main rf resonator of the fRC temporarily installed in the E4 experimental room. The resonator is divided into upper and lower parts.

Figure 3.2.7. Photograph of the acceleration gap of the main resonator.

3.3 IRC

Outline

The IRC is a room temperature ring cyclotron with K-980 MeV and located upstream of the SRC. The injector of the IRC is the RRC or the fRC. The beam energy extracted from the IRC is shown in Fig. 3.3.1. The abscissa indicates charge to mass ratio q/A. The maximum energy is 127 MeV/nucleon. Main parameters of the IRC are listed in Table 3.3.1. A plan view of the IRC is shown in Fig. 3.3.2. The IRC consists of four sector magnets, beam injection and extraction elements, two acceleration and one flattop rf resonators, and some kinds of beam diagnostic instruments. The average radii of the injection and the extraction are 2.77 m and 4.15 m, respectively. Acceleration rf frequency is from 18.0 MHz to 38.2 MHz according to the energy of the accelerated ions.

Sector magnets

The sector magnets of the IRC were designed based on those of the RRC. Fundamental structure of the poles and yokes is a stack of low carbon steel plates with a thickness of 260 mm or 280 mm. Carbon content of the steel is typically 0.002%.

Main parameters of the sector magnets are listed in Table 3.3.2. The main coils of the sector magnets are designed to be of a low power consumption type. The maximum power consumption of the main coils is suppressed at 70% of that of the RRC, although the maximum magnetic field is higher than that of the RRC. Temperature rises of cooling water by the main coils are less than 10 degrees. Twenty pairs of trim coils are mounted on the pole surface. The arrangement of the trim coils is shown in Fig. 3.3.3. Vacuum in the trim coil area is separated from that for the beams by thin stainless steel plates with a thickness of 4 mm. Electric insulation of the trim coils is done by flash-coated with fused aluminum oxide. The vacuum chamber and the upper and lower poles with the trim coils mounted are integrated as shown Fig. 3.3.4, to simplify the assembling of the sector magnet at the RIKEN site. Thirty-eight switching power supplies in total are used for the excitation of the trim coils. The innermost three and the outermost three trim coils are excited independently among the sector magnets. Average temperature of the cooling water for trim coils will be precisely controlled in order to achieve good stability of the magnetic field.

In 2001, two sector magnets were assembled and aligned at the factory and the magnetic field mapping of the two sector magnets was measured. Figure 3.3.5 shows a photograph of the sector magnets and the magnetic field mapping device that were taken at the factory. The whole system of the IRC has already been installed and assembled in the IRC vault; a photograph of the sector magnets together with the rf resonators and so on is shown in Fig.

3.3.6.

Injection and extraction system

The injection system consists of one electrostatic inflection channel (EIC), two magnetic inflection channels (MIC1 and MIC2), one bending magnet (BM1) and two quadrupole magnets. The extraction system consists of one electrostatic deflection channel (EDC), two magnetic deflection channels (MDC1 and MDC2) and two bending magnets (EBM1 and EBM2). Table 3 shows parameters of the injection and extraction devices. The MIC1 and MIC2 are equipped with iron shims with thickness of 2.2 mm and 5 mm, respectively. On the other hand, the MDC1 and the MDC2 are air-cored coils. All magnetic channels are installed in the 52-mm gap of beam vacuum in the sector magnets. The material of septum for the EIC is stainless steel. For the EDC, copper is used in consideration of heat load. Figure 3.3.7 shows a photograph of the entrance of the EDC. Gap width of the EIC and the EDC is 12 mm. Power supplies of 120 kV are prepared. For usual use, 80 kV/cm is enough for both electrostatic channels. It is noted that a voltage of 120 kV or an electric field of 100 kV/cm was applied successfully in a test at the factory.

Rf resonators

Two kinds of resonators are adopted for the IRC: two main resonators and one flattop resonator. A schematic drawing of the acceleration one is shown in Fig. 3.3.8. The main resonators are of a single-gap type with flapping panels for changing resonant frequency. This type of resonator has a large advantage in that the area of sliding rf contact can be minimized. The maximum voltage is supposed to be 600 kV for one resonator. The flattop resonator is of a single-gap type with shorting plates. The resonant frequency is coarsely varied from 18 MHz to 40.5 MHz by adjusting the flapping-panels from 0^o to 90^o and is finely tuned with a ratio of more than 0.5% inserting the block tuners. The estimated current density on the sliding contact which is adopted to the connection between flapping-panels and the cavity wall is less than 60 A/cm. The rf power is fed by an inductive loop whose coupling strength can be varied changing the cross section of the loop to obtain an impedance matching to 50 Ω. The resonator wall consists of an oxygen-free copper board with a thickness of 4 mm, 25 mm space gap, and a stainless-steel board with a thickness of 45 mm. In order to reduce the out-gas into the inside of the resonator, the space between the walls is differentially pumped using turbo-molecular pumps. The thickness of the stainless-steel wall is decided so as to make the deformation due to the pressure of the atmosphere less than 1.5 mm. The water channels attached to the copper wall utilizing 25 mm space gap are arranged based on the heat calculation. The heat density distribution is obtained using MAFIA. The final amplifiers are

the same as those for the fRC; they are based on a tetrode (SIEMENS RS2042SK) with a grounded-grid circuit.

Vacuum system

The vacuum system is shown in Fig. 3.3.9. The main vacuum pumping equipment consists of 12 cryopumps with 10,000 L/sec, 2 cryopumps with 4,000 L/sec and four turbo-molecular pumps with 3,200 L/sec. The required pressure is about $1x\ 10^{-6}$ Pa. Eight turbo-molecular pumps with 350 L/sec are used for differential pumping of the main resonators.

Beam diagnostics

The beam diagnoatic system consists of two main differential probes (MDP1 and MDP2), two injection radial probes (IRP1 and IRP2), two extraction radial probes (ERP1 and ERP2) and one phase probe. Strokes of MDP1 and the MDP2 are 2.7 m and 2.4 m, respectively. Moving speed of the probes is designed to be 2 m/min. The beam sensor part of IRP2 is of a block type, and those of the IRP1 and ERPs are of a wire type with three tungsten filaments. The phase probe is equipped with sixteen pairs of electrodes.

Table 3.3.1. Main parameters of the IRC.

K-value	980
Number of sector magnets	4
Harmonics	7
Injection radius	2.77 m
Extraction radius	4.15 m
Velocity gain	1.5
Maximum energy	127 MeV/nucleon
Maximum magnetic rigidity	4.57 Tm
Number of rf resonators	
Main acceleration	2
Flattop	1
Rf frequency	
Main acceleration	18.0-38.2 MHz
Flattop	72.0-114.6 MHz

Table 3.3.2. Main parameters of the sector magnets.

Pole gap	80 mm
Sector angle	53 degree
Purcell gap	1 mm
Total weight	2800 ton
Height	5.2 m
Maximum magnetic field	1.9 T
Main coil	
Maximum current	450 A
Maximum excitation current	178 kA/sector
Current stability	2×10^{-5}
Power consumption (total)	330 kW
Trim coil	
Number of trim coils	20 pairs/sector
Maximum current	400, 500, 600 A
Current stability	5×10^{-4}
Power consumption (total)	180 kW

Table 3.3.3. Parameters of the beam injection and extraction devices.

Magnetic devices			
Device	Bend angle (deg)	Radius (m)	B (T)
BM1	105	1.65	1.82
MIC1	30	1.53	0.12
MIC2	60	1.43	0.25
MDC1	20	2.55	-0.07
MDC2	35	2.63	-0.12
EBM1	13	3.3	1.43
EBM2	32	2.8	1.68
Electrostatic deflector			
Device	Length(m)	gap (mm)	E(kV/cm)
EIC	0.7	12	100
EDC	1.3	12	100

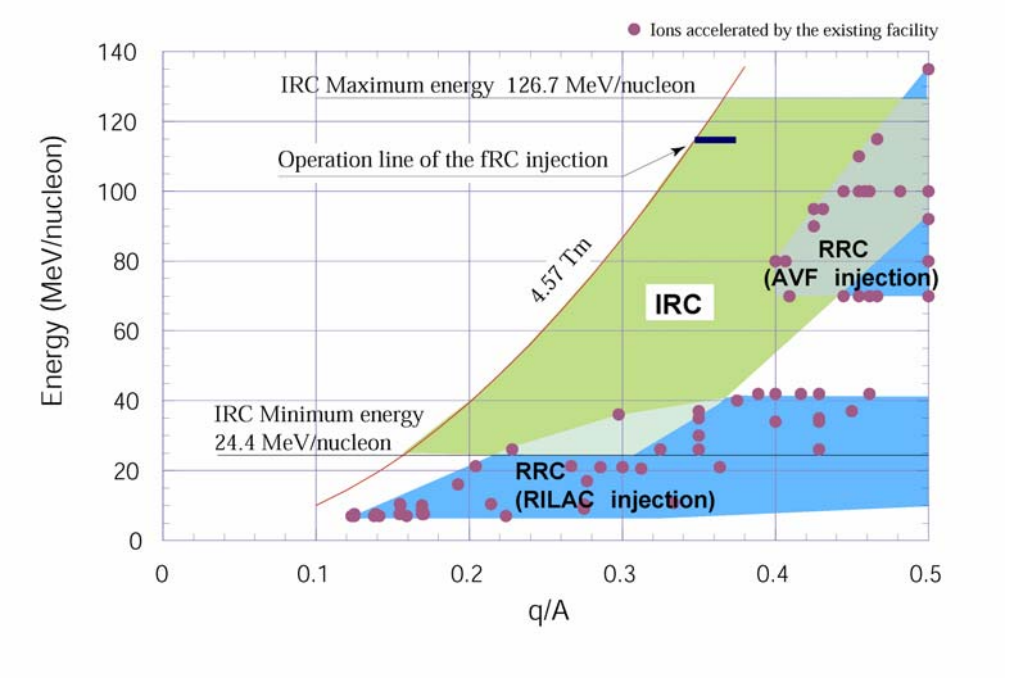

Figure 3.3.1. Beam energy of the IRC.

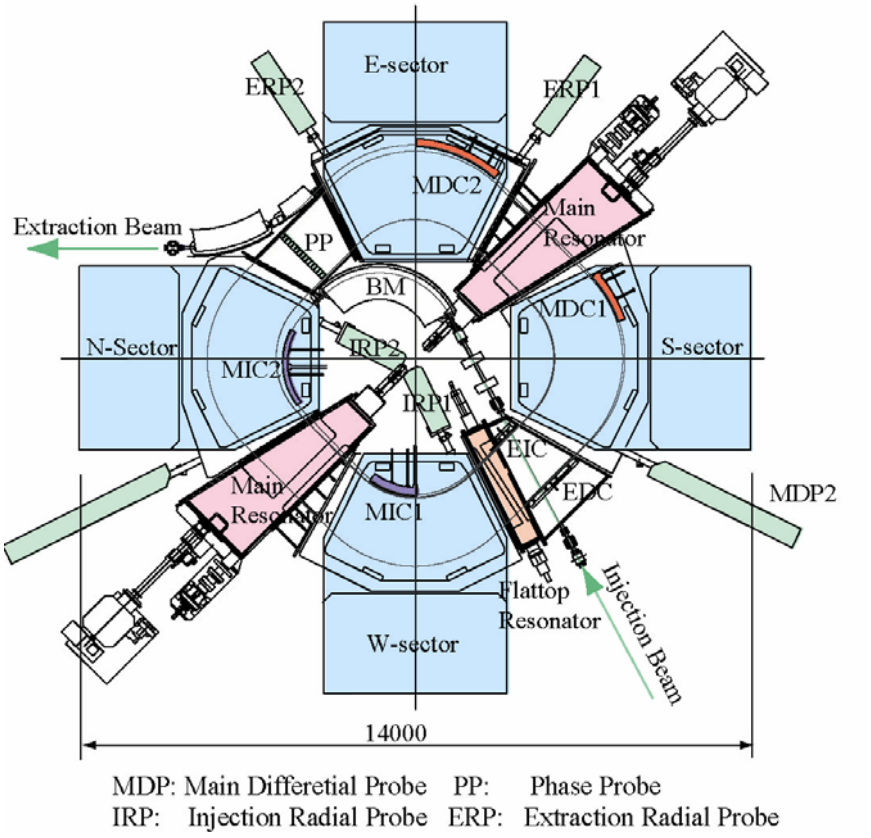

Figure 3.3.2. Plan view of the IRC.

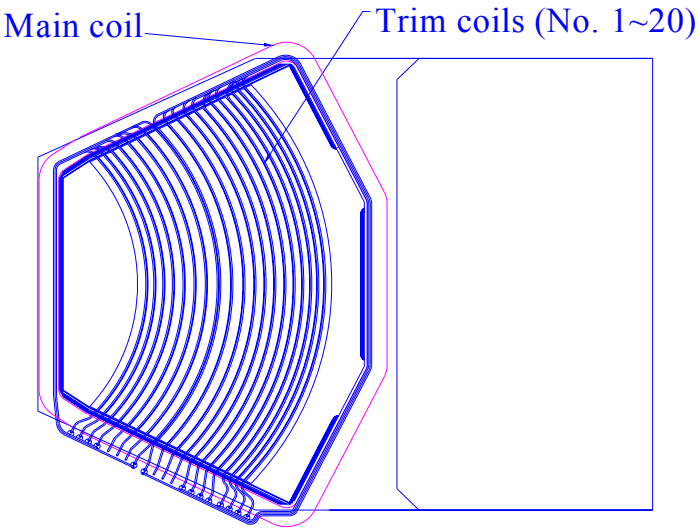

Figure 3.3.3. Arrangement of the main coil and the trim coils.

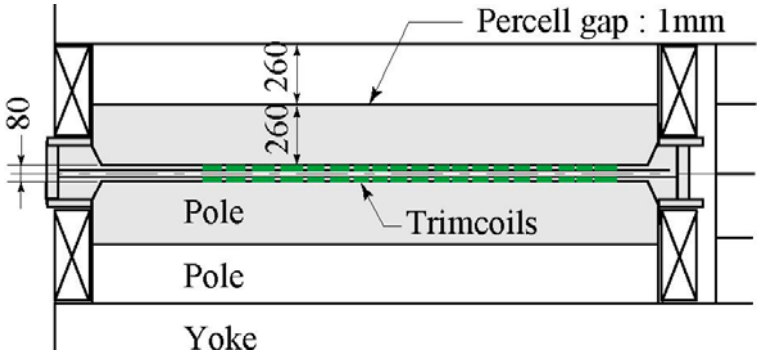

Figure 3.3.4. Cross-section of the poles and the beam chamber of the sector magnet.

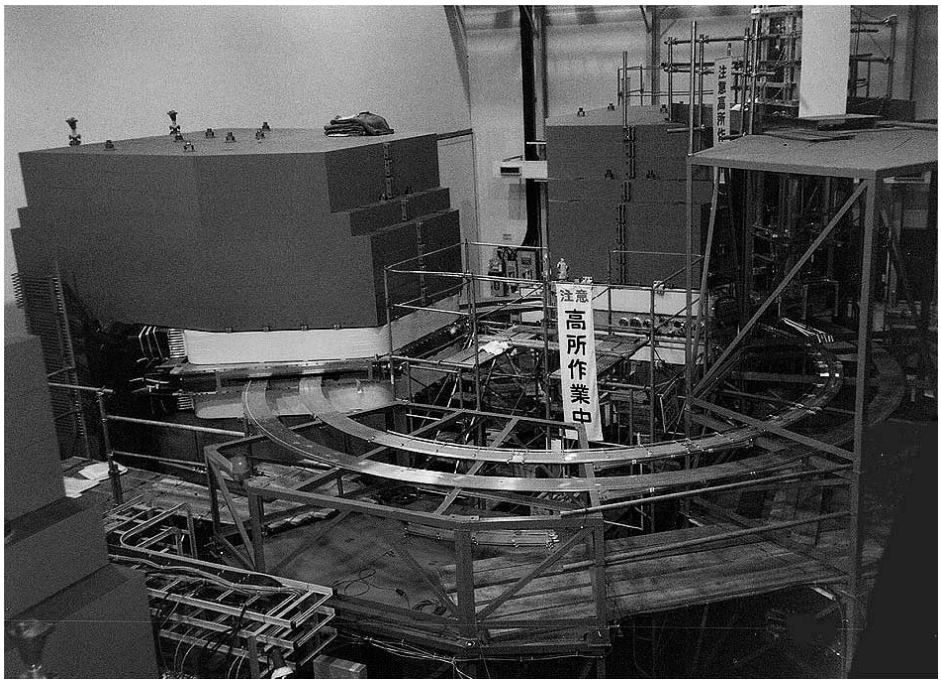

Figure 3.3.5. Photograph of the two sector magnets and the magnetic field mapping device at the factory.

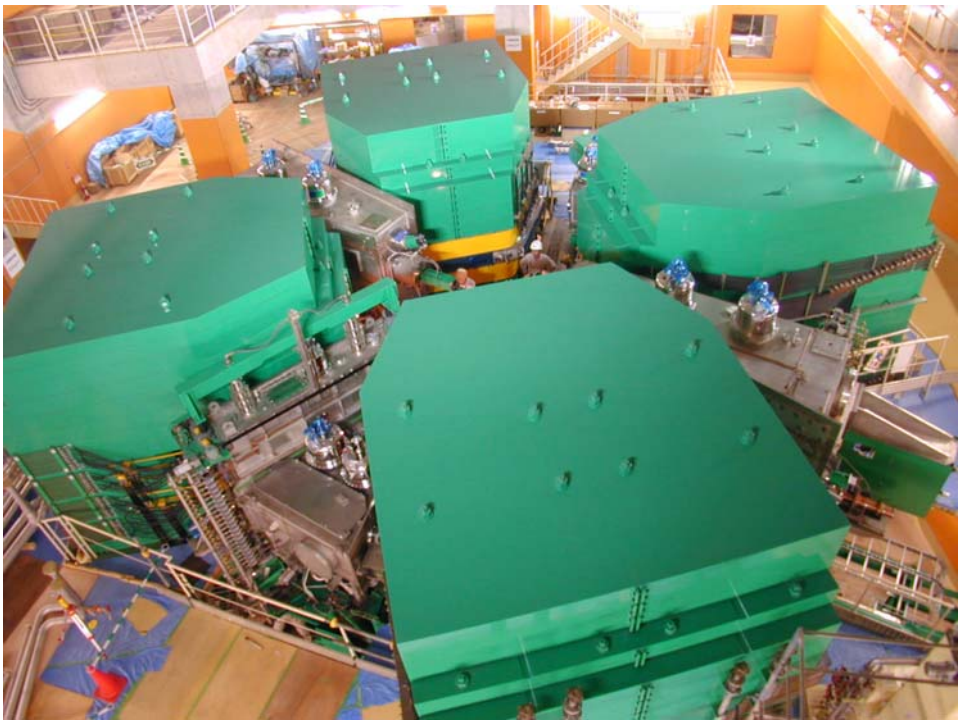

Figure 3.3.6. Photograph of the IRC in the IRC vault.

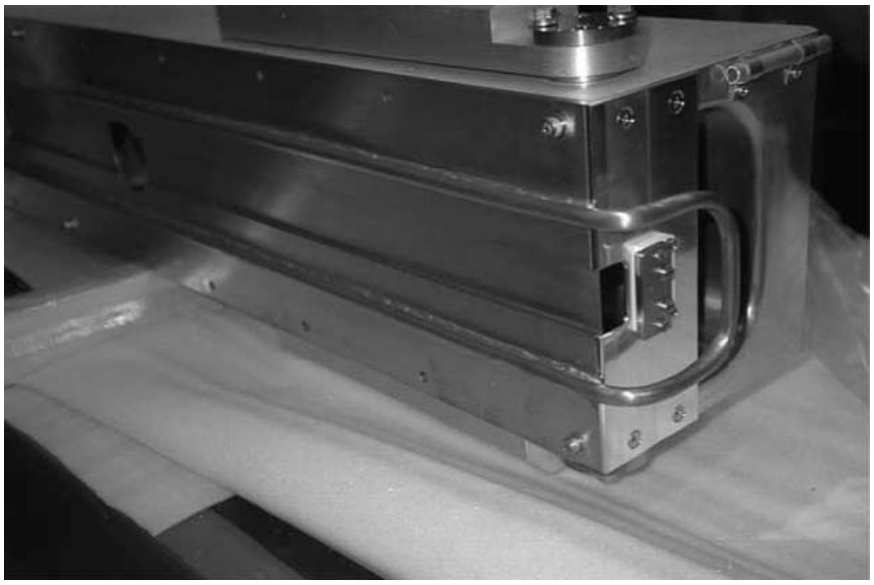

Figure 3.3.7. Photograph of the EDC.

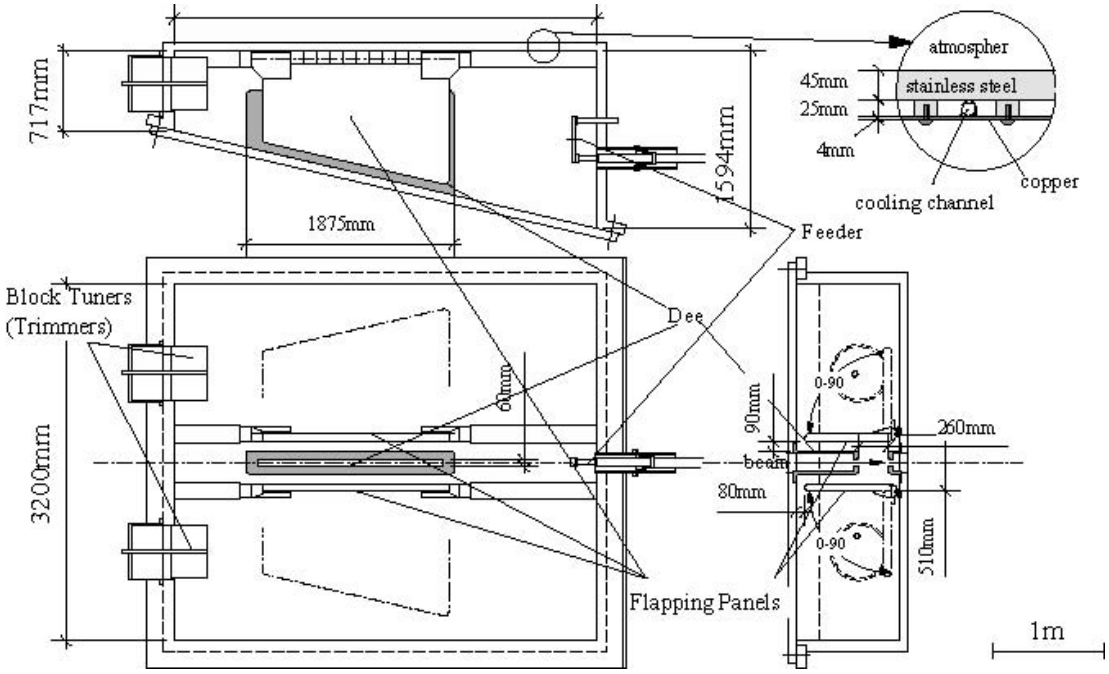

Figure 3.3.8. Schematic drawing of the acceleration rf resonator.

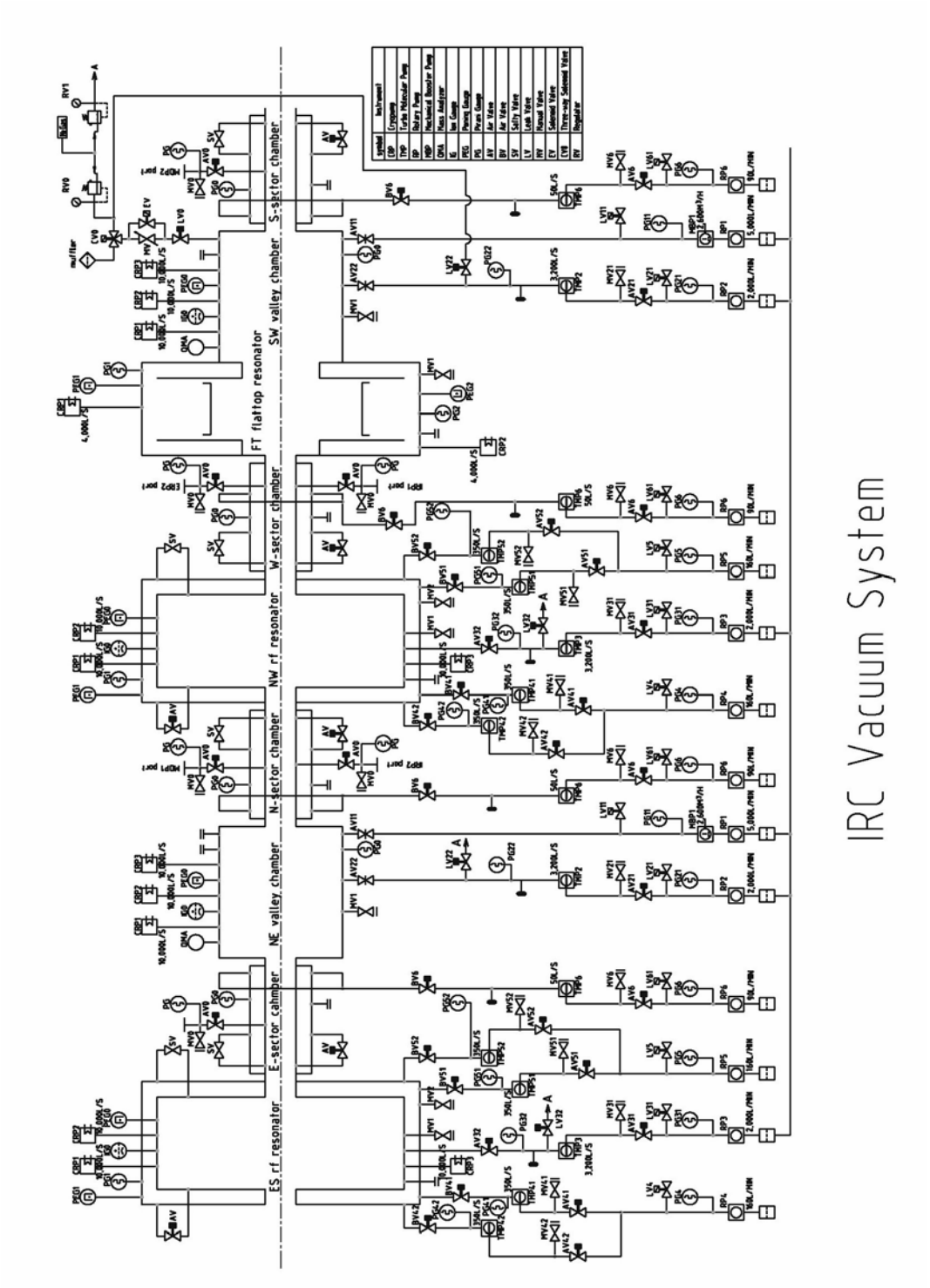

Figure 3.3.9. Vacuum system.

3.4 SRC

Outline

The SRC is the final-stage accelerator of a cascade of ring cyclotrons for the RIBF; it is a superconducting ring cyclotron with K-2500 MeV. The beam energy extracted from the SRC is shown in Fig. 3.4.1. Main parameters of the SRC are listed in Table 3.4.1. A bird's eye view and a plan view of the SRC are shown in Fig. 3.4.2 and Fig. 3.4.3, respectively. The SRC consists of six superconducting sector magnets, beam injection and extraction elements, four acceleration and one flattop rf resonators, and some kinds of beam diagnostic instruments. The average radii of the injection and the extraction are 3.56 m and 5.36 m, respectively. Acceleration rf frequency is from 18.0 MHz to 38.2 MHz according to the energy of the accelerated ions. The total weight of the SRC is 8,300 t.

We have made the significant design change of the sector magnets from the original open-structure with active magnetic shields to the present iron-covered structure. In this design, the iron pole of the sector magnet can be placed at the room temperature (in the original design the pole is placed at 4.5 K). Now the SRC is of self magnetic-flux and radiation leakage-shielding structure. In addition, this iron-cover produces the following effective results: (1) We do not need any extra non-magnetic local radiation shielding of the concrete blocks as big as 3 m cubes. (2) The stray field in the valley (whose flux direction is opposite to that of the sector field) is reduced from 0.5 T to 0.04 T (at maximum). This gives us the merits: (2-1) The maximum sector field needed is reduced. (2-2) The maximum magnetomotive force required is also reduced. (2-3) The maximum stored energy and the electromagnetic forces exerted onto the main coil are significantly reduced. (2-4) We need not use superconducting magnetic channels for the beam injection and extraction that are very difficult to fabricate. Now all the injection and extraction magnetic channels are normal with the moderate power consumption and their structures are very similar to those for the RRC and the IRC. (2-5) The shift of the injection and extraction trajectory depending on the negative stray field strength is greatly reduced (almost no shift.) This significantly facilitates the design of the injection and extraction system. Now we have only one superconducting magnet of small size for the beam injection, SBM. (2-6) We use the rf cavities and valley chambers having the structures with small modifications to those of the IRC because of the low stray field. (3) The stray field outside the SRC is reduced to a few gauss. We need neither the active magnetic shielding difficult to fabricate nor the thick iron plates enclosing the huge SRC vault. (3-1) We place the rf oscillators near the SRC like the RRC and the IRC. (3-2) The SRC vault is now very safe for working people even inside the SRC. (4) Reducing the cold mass by placing the pole at the room temperature significantly shortens the cooling time.

Simulation on space charge limit

A numerical simulation study on the longitudinal space charge (LSC) effects of heavy-ion beams was carried out in order to know limits in extracted beam current due to these effects.

Three-dimensional multi-particle simulation code "NAJO" [A. Chabert et al., Proc. Conf. Accelerator Design and Operation, Berlin, Germany, 1983-9 (Springer-Verlag, 1984), p.164.] was used for these simulations under realistic conditions. The simulations were made for $^{16}O^{8+}$ ions and $^{238}U^{88+}$ ions. The starting point for particles was set at the innermost radius and center of the valley where the SBM is placed. The central particle of the beam was given initial parameters corresponding to the accelerated equilibrium orbit (AEO).

For the $^{16}O^{8+}$ beam, ions were accelerated to the desired final beam energy with ~ 276 turns. The turn separation for the central beam was ~ 4.5 mm at the EDC. In order to get larger turn separation at the extraction radius, a precessional motion was introduced by initially giving the beam a small angle at the starting point. The off-centered beam (with the deviation of +6 mrad from the AEO at the starting point) yielded the turn separation of 10.6 mm at the extraction radius. Under these conditions the beam clearance between the last two turns was 2.3 mm at the level of 0.1 % as shown in Fig. 3.4.4, in which the widening of the radial beam size due to the LSC effect is also shown. The maximum allowable intensity for the $^{16}O^{8+}$ beam was estimated to be ~ 9 pμA as shown in Fig. 3.4.5. The intensity limit is defined by the beam intensity when the particle loss due to the radial widening is 1 %. While the thickness of the septum of the EDC is ~ 0.5 mm, the beam clearance between the last two turns should be larger than the thickness because of the shadow of the septum. Compensation of the LSC effect by the flattop acceleration (FT) allowed us to increase this intensity limit up to ~ 20 pμA as shown in Fig. 3.4.5.

For the $^{238}U^{88+}$ beam, it was necessary to perform 321 turns to reach the desired final energy. The turn separation of the centered beam was 3.6 mm at the extraction radius. Off-centered injection with the deviation of -2 mm and +6 mrad from the AEO allowed us to get the turn separation of 10.8 mm at the extraction radius. Under these conditions the beam clearance between the last two turns was ~ 3 mm at the level of 0.1 %. The maximum allowable intensity for the $^{238}U^{88+}$ ion beam was estimated to be ~ 1.8 pμA as shown in Fig. 3.4.6. Compensation of the LSC effect by the FT allowed us to increase this intensity limit up to ~ 2.1 pμA.

Sector magnets

Main parameters of the sector magnets are listed in Table 3.4.2. The assembling of the whole sector magnets has already been completed. The cool-down of them started this

September and is now being carried out. We plan to start the magnetic field mapping immediately after the temperature of the magnets will reach 4.5 K. For the details of the sector magnets, refer to Chapter 4 (“Status of the superconducting magnets for the SRC”).

Injection and extraction system

The injection system consists of one superconducting bending magnet (SBM), two normal-conducting magnetic inflection channels (MIC1 and MIC2), and one electrostatic inflection channel (EIC). The extraction system consists of one electrostatic deflection channel (EDC), three normal-conducting magnetic deflection channels (MDC1, MDC2 and MDC3), and one normal-conducting bending magnet (EBM). Table 3.4.3 shows parameters of the injection and extraction devices.

Since the beams are designed to inject crossing the EIC and EDC (see Fig. 3.4.7), their respective electrodes have a hole for that purpose. To minimize the diameter of the hole, each trajectory is adjusted with several steering magnets (see Fig. 3.4.8) so that the beam passes on the centers of these two holes as closely as possible. Because of the difference between various beam orbits caused by the stray magnetic field in the valley, the EIC and EDC s hould be movable in the radial direction by 18 mm and 31 mm, respectively. Furthermore, the radius of curvature should be adjustable to fit various beam trajectories; the EIC and EDC consist of three arcs connected with two hinges, respectively. Gap width of the EIC and the EDC is 12 mm. The required electric fields are 100 kV/cm for both electrostatic channels. The MIC1 (see Fig. 3.4.9), MDC1 and MDC2 are installed in the gap of 90 mm of the beam chamber of the sector magnets, while the MIC2 and MDC3 are installed in the atmospheric rooms, the inner height of which is 140 mm. The MIC1 and MDC2 have cross-sectional structures similar to those of the IRC. The required fields of the MIC2 and MDC3 are considerably higher than those of conventional ring cyclotrons. Because of the required high field and limited available space, the SBM should be a superconducting magnet (the details are described in Chapter 4 (“Status of the superconducting magnets for the SRC”). The EBM (see Fig. 3.4.10) was designed to be a single magnet with a long arc of 3.6 m. So, two pairs of steering coils are built in the EBM to adjust beam trajectories.

Rf resonators

The SRC has four main resonators and one flattop resonator. The resonators are placed in the valley regions surrounded by the upper, lower and side walls of the magnetic shield. The structure of these resonators are similar to those of the IRC; the main resonators are of a single-gap type with flapping panels for changing resonant frequency, and the flattop resonator is of a single-gap type with shorting plates. The required frequency is from 18 MHz

to 38.2 MHz. The maximum voltage is supposed to be 600 kV for one resonator. The power dissipation is estimated, from the measurement of electrical characteristics at the factory, to be 120 kW at 38.2 MHz with a gap voltage of 600 kV. The final amplifiers are the same as those of the fRC and IRC; they are based on a tetrode (SIEMENS RS2042SK) with a grounded-grid circuit. Figure 3.4.11 and 3.4.12 show a schematic drawing and a photograph of the resonators, respectively.

Vacuum system

The main vacuum pumping equipment for the evacuation of the beam chamber consists of 16 cryopumps with 10,000 L/sec, two cryopumps with 2,400 L/sec, four turbo-molecular pumps with 3,200 L/sec and eight turbo-molecular pumps with 330 L/sec. The required pressure is in the order of 10^{-6} Pa.

Beam diagnostics

The beam diagnostic system is similar to that of the IRC. It consists of a main differential probe, two extraction radial probes and a phase probe. The phase probe is equipped with twenty pairs of electrodes.

Table 3.4.1. Main parameters of the SRC.

K-value		2,500
Number of sector magnets		6
Harmonics		5, 6
Injection radius		3.56 m
Extraction radius		5.36 m
Velocity gain		1.51
Maximum energy	^{238}U	350 MeV/nucleon
	^{48}C	400 MeV/nucleon
	d	880 MeV
Maximum magnetic rigidity		8.5 Tm
Number of rf resonators		
Main acceleration		4
Flattop		1
Rf frequency		
Main acceleration		18.0-38.2 MHz
Flattop		72.0-114.6 MHz

Table 3.4.2. Main parameters of the sector magnets.

Pole gap	714 mm max.
Sector angle	25 degree
Total weight	8,300 ton
(incl. magnetic shields)	
Height	6 m
Maximum magnetic field	3.8 T
Main coil	
Maximum current	5,200 A
Maximum excitation current	4 MA/sector
Current stability	1×10^{-5}
Trim coil	
Number of trim coils	4 blocks (super)
	22 pairs (normal)
Maximum current	3,200 A (super)
	600, 800, 1,200 A (normal)
Current stability	1×10^{-4}
Power consumption (total)	1,100 kW

Table 3.4.3. Parameters of the beam injection and extraction devices.

Magnetic devices

Device	Bend angle (deg)	Radius (m)	B (T)
SBM	82	1.21	3.77
MIC1	50	1.36	0.29
MIC2	74	1.20	0.96
MDC1	13	2.20	-0.07
MDC2	37	2.32	-0.20
MDC3	41	2.5	-0.54
EBM	55	3.8	2.04

Electrostatic deflector

Device	Length(m)	gap (mm)	E(kV/cm)
EIC	1.3	12	100
EDC	2.2	12	100

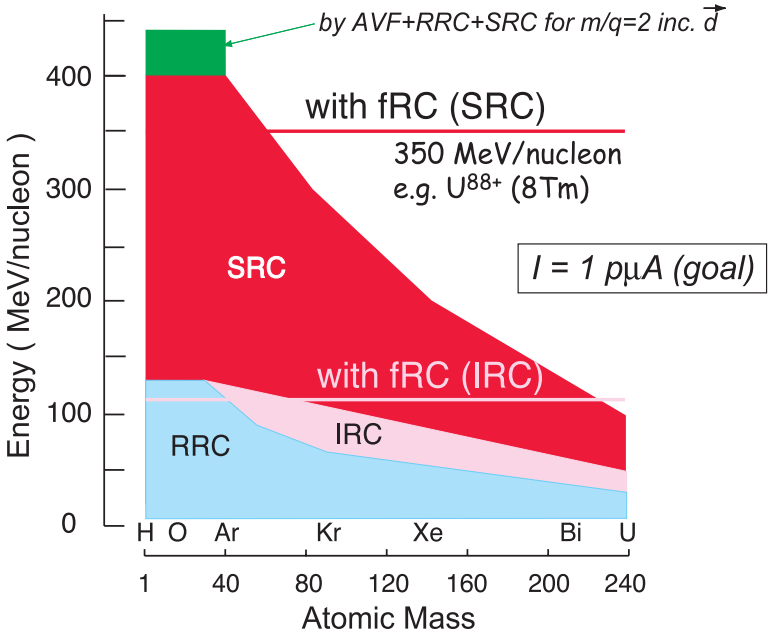

Figure 3.4.1. A diagram of the RIBF acceleration performance (MeV/nucleon) for each atomic mass.

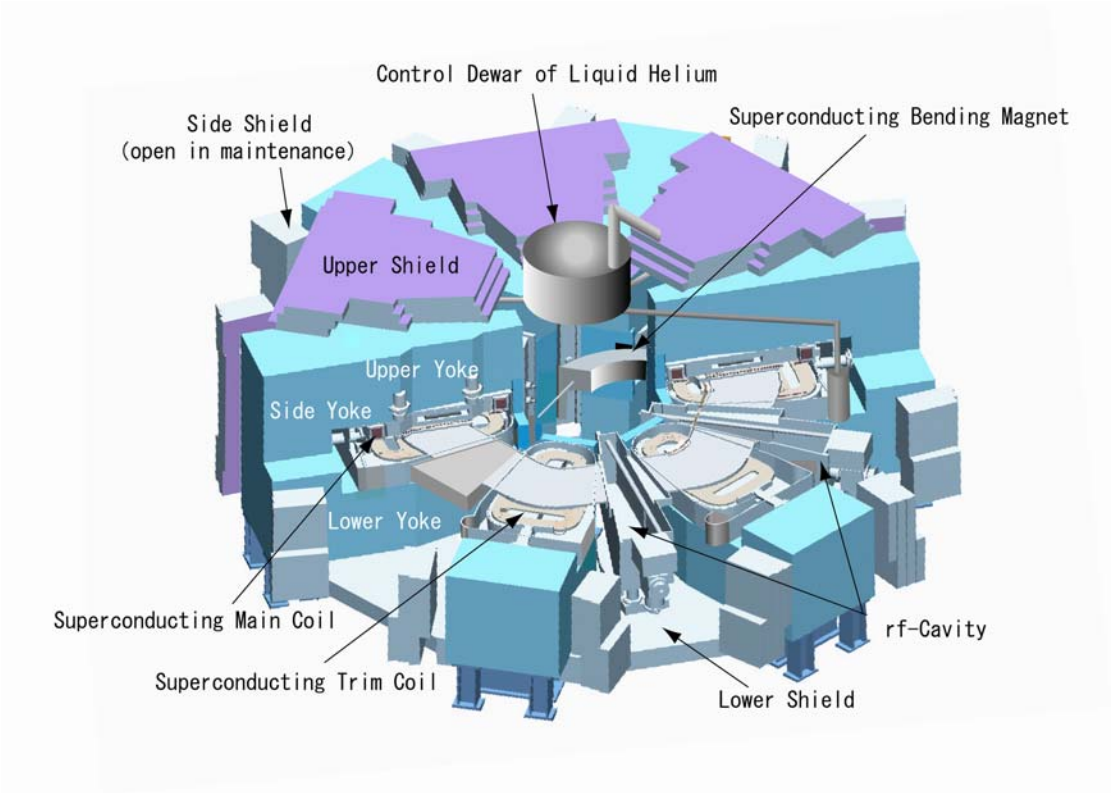

Figure 3.4.2. Bird's eye view of the SRC.

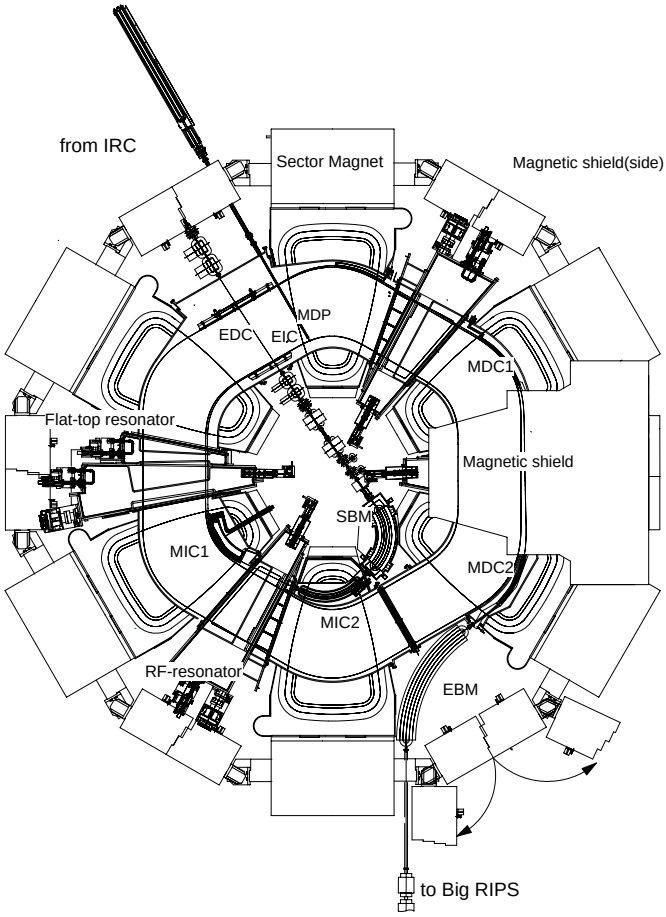

Figure 3.4.3.a. Plan view of the SRC.

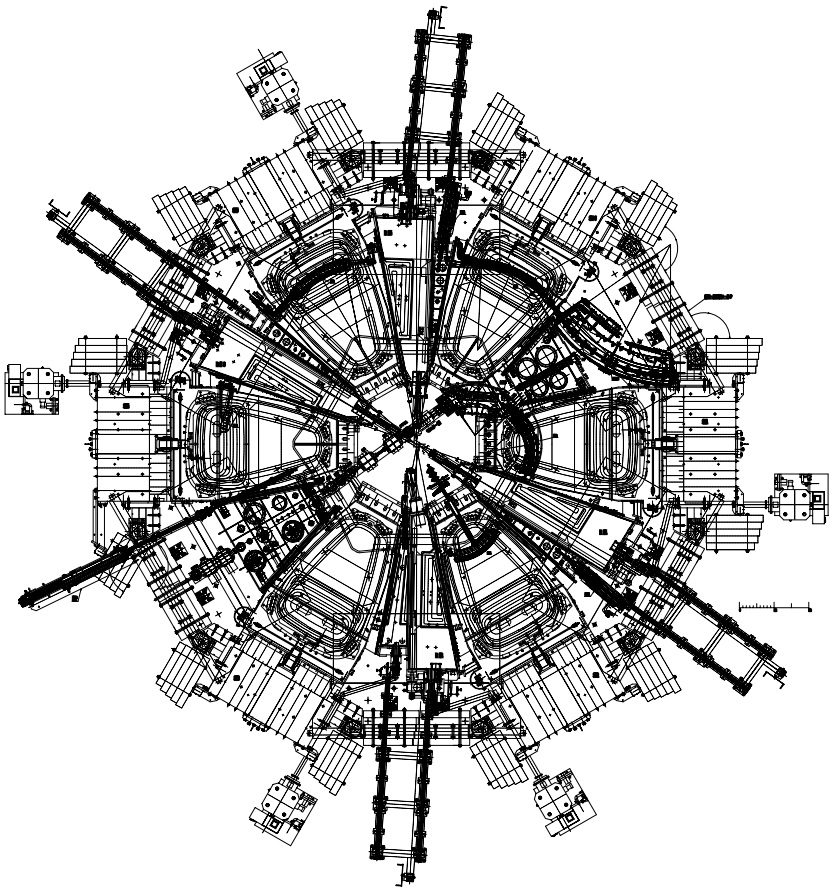

Figure 3.4.3.b. Drawing of a plan of the SRC.

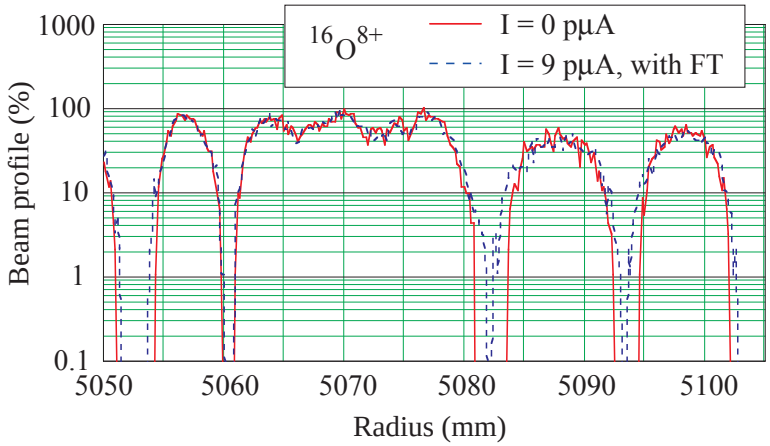

Figure 3.4.4. Radial turn pattern for the $^{16}O^{8+}$ ions obtained with off-centering. Solid line: I = 0 pμA, and dash line: I = 9 pμA with the FT.

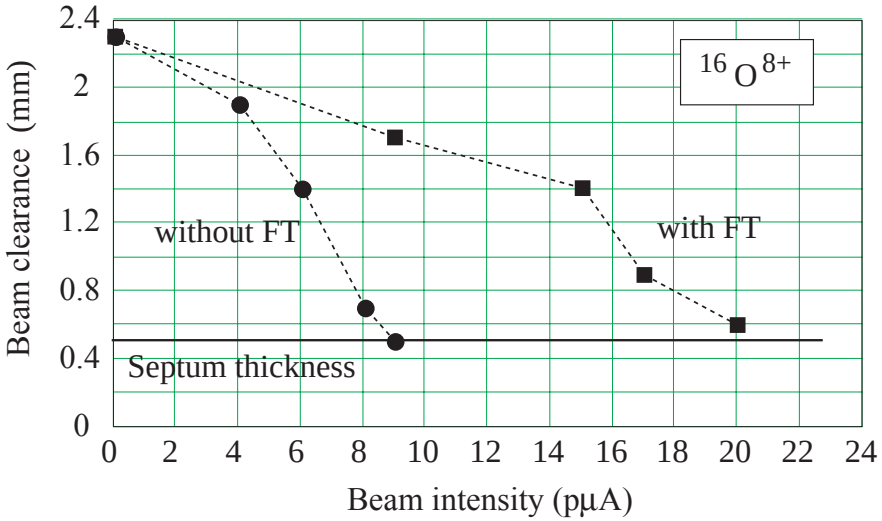

Figure 3.4.5. Beam clearance between the last two turns as a function of beam intensity for the $^{16}O^{8+}$ beam.

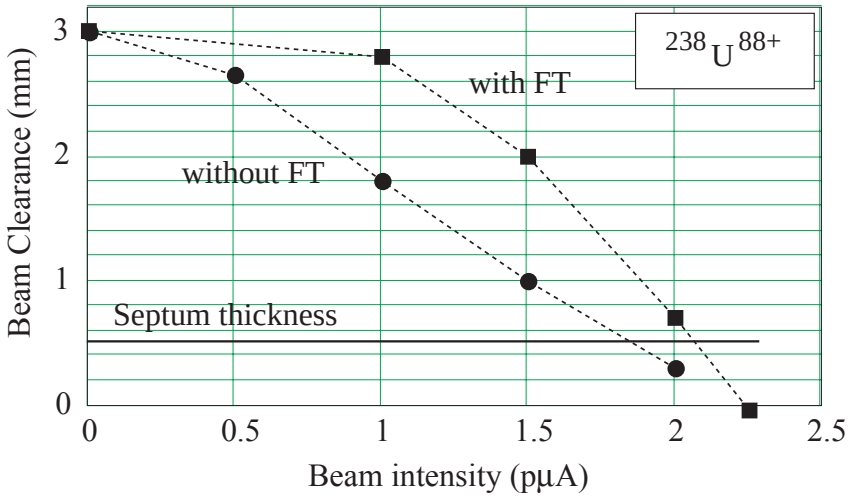

Figure 3.4.6. Beam clearance between the last two turns as a function of beam intensity for the $^{238}U^{88+}$ beam.

Figure 3.4.7.a. Photograph of the EDC.

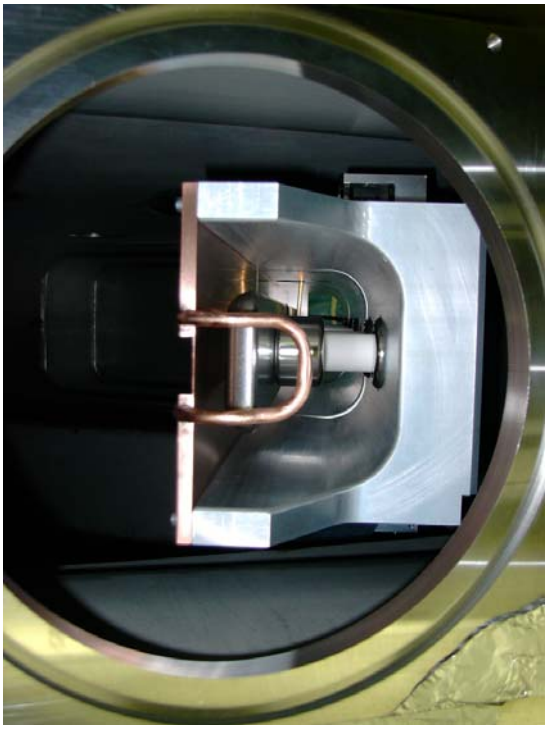

Figure 3.4.7.b. Photograph of close-up view of the electrodes of the EDC.

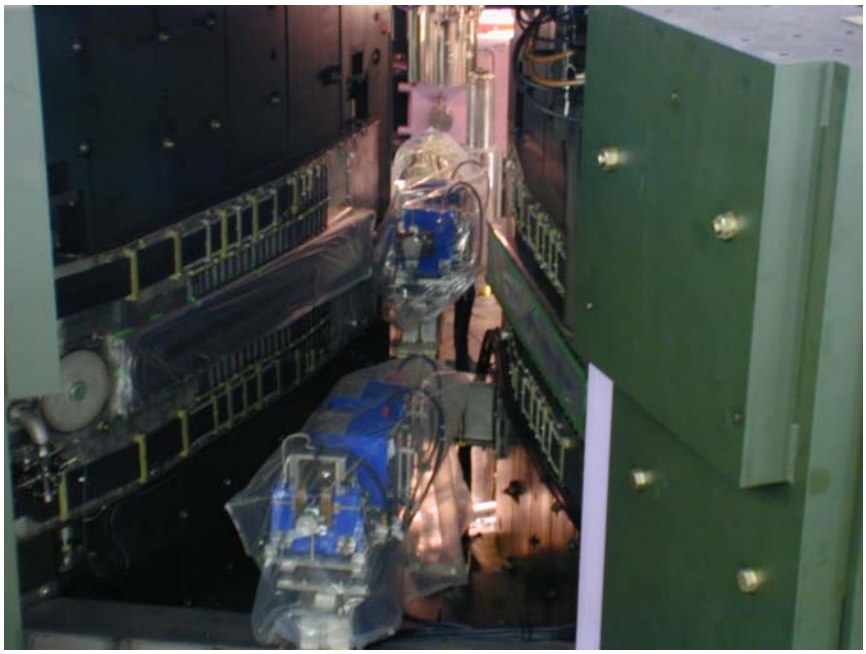

Figure 3.4.8. Photograph of the steering magnets to finely adjust the beam injection trajectory.

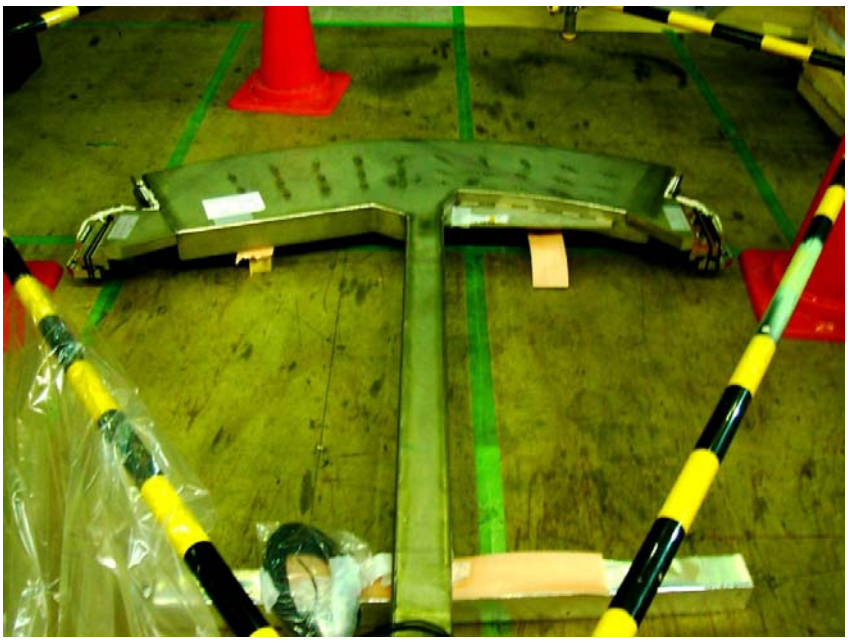

Figure 3.4.9. Potograph of the MIC1.

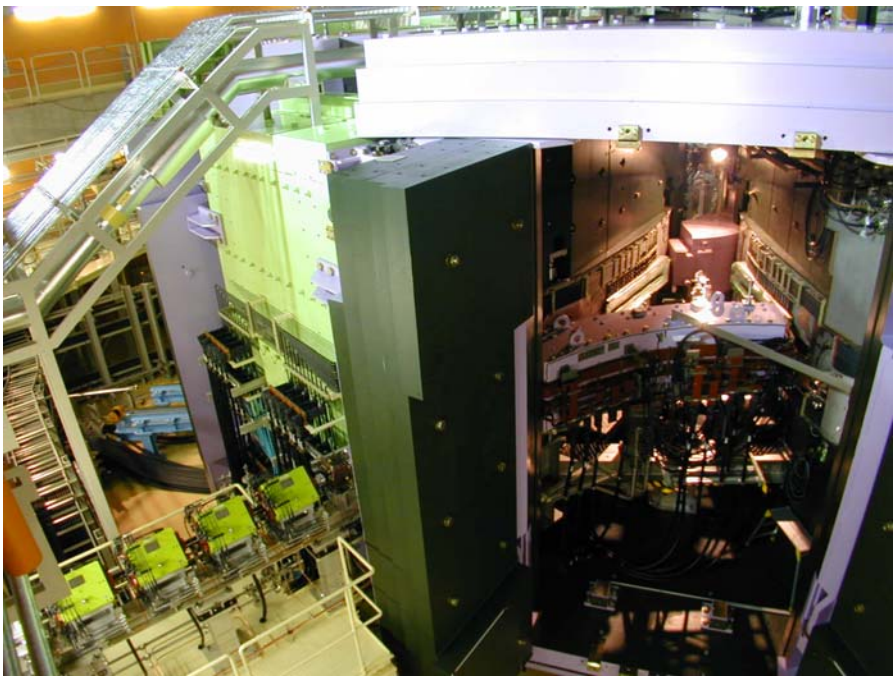

Figure 3.4.10. Photograph of the EBM installed in the SRC.

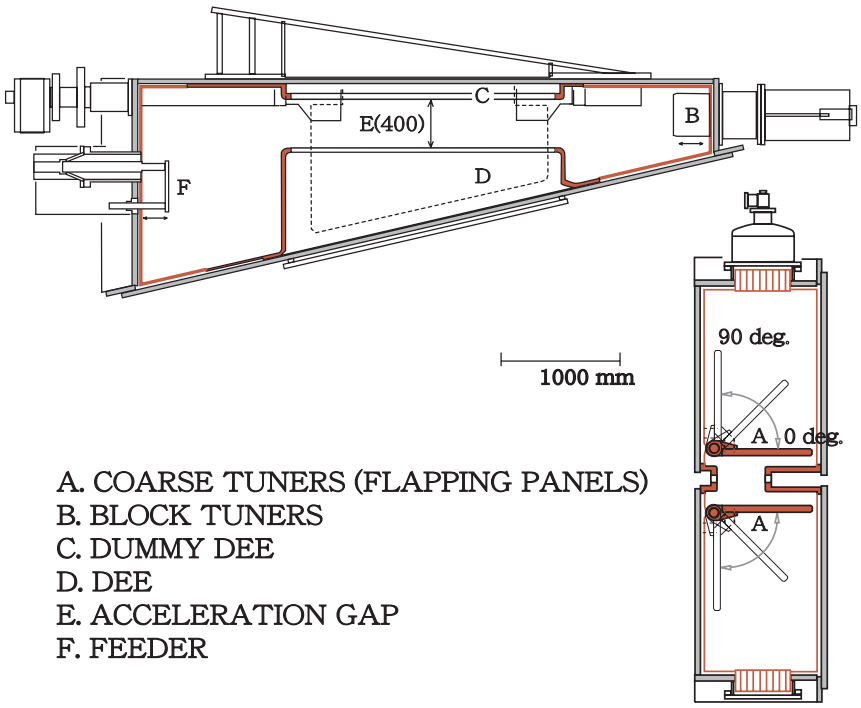

Figure 3.4.11. Schematic drawing of the main resonator.

Figure 3.4.12. Photograph of the main resonators.

3.5 Beam transport system

In the RIBF, there are many long beam lines that intricately connect the RRC, fRC, IRC, SRC and BigRIPS as shown in Fig. 1 in Chapter 1 ("Overview of the RIBF Project"). Among them, the beam lines from the IRC to the SRC as well as from the SRC to the BigRIPS have already been completed. The installation of the beam lines from both the RRC and the fRC to the IRC will be carried out during the period of February-May in 2006. The beam line from the IRC back to the RARF facility, which is necessary for the simultaneous utilization of the beams from the IRC at both the RARF and the RIBF, is planned to construct in 2007. Photographs of the installed beam transport lines are shown in Figs. 3.5.1, Fig. 3.5.2 and Fig. 3.5.3.

A beam rebuncher for the beam line between the RRC and the fRC is being designed for completion in May 2006. It is operated at 110 MHz, which is six times that of the RRC or twice that of the fRC. By use of the rebuncher, the phase width of the beam at the injection point of the fRC can be 20^{o}, which is well within the flat region of the flattop voltage of the fRC. A cutaway view of the rebuncher designed is shown in Fig. 3.5.4. The diameter and length of the resonator are 900 mm and 1000 mm, respectively. The number of gaps is four. The stem of the center drift tube is perpendicular to that of its neighboring two drift tubes. The required voltage per gap of about 30 kV will be achieved with a power consumption of 600 W

Figure 3.5.1. Photograph of the extraction beam line from the IRC.

Figure 3.5.2.a. Photograph of the beam transport line between the IRC and the SRC, seen from the upstream.

Figure 3.5.2.b. Photograph of the beam transport line between the IRC and the SRC, seen from the downstream.

Figure 3.5.3. Photograph of the beam transport line between the SRC to the BigRIPS.

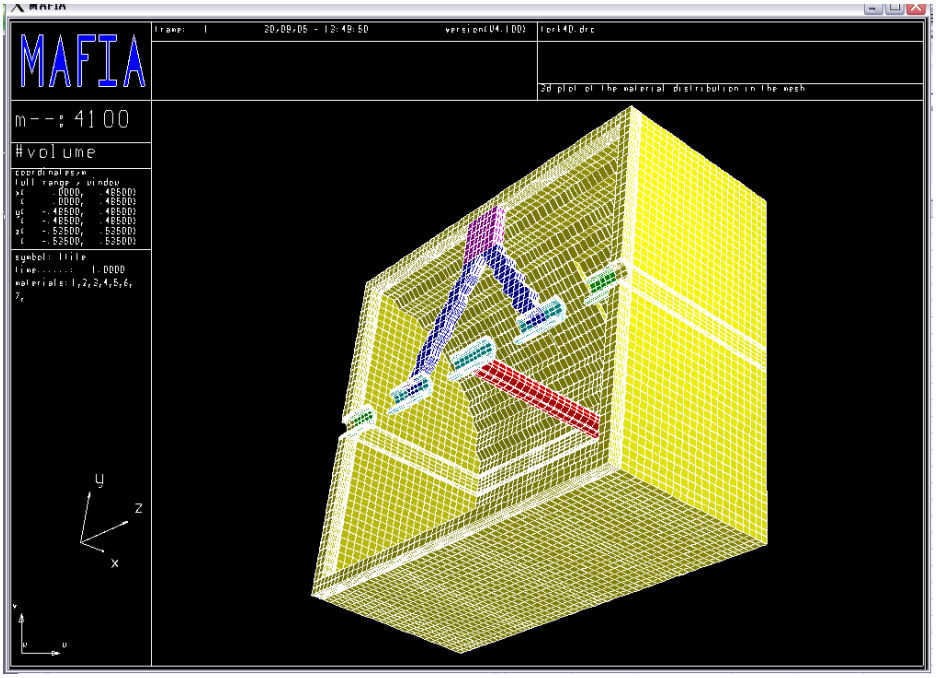

Figure 3.5.2. Schematic of the designed rebuncher between the RRC and the fRC. Half part of the resonator is shown.

3.6 Control system

The RARF control system is based on a CAMAC serial crate network and is supported by two types of modules, communication interface modules (CIMs) and device interface modules (DIMs). These modules were originally developed by RIKEN about twenty years ago in order to assist the main computer in its tasks. The CIM is a CAMAC module that has twelve pairs of serial I/O ports, and it executes the message transfer between the VME and the DIM. The DIM has 32 DI/DO ports and 16 AI ports, and it executes a local sequence control, local surveillance, function generation and testing. Information is transferred serially between these two modules through a pair of plastic optical fiber cables. Almost all magnet power supplies and beam diagnostic devices are controlled by them. Other control devices are also used in the RARF: a GP-IB, a network I/O (NIO) system, and a programmable logic controller (PLC) and a network-DIM (N-DIM). The GP-IB controls mainly measurement instruments such as a vector-voltmeter and 20-year-old power supplies in the RILAC.

The EPICS has been running on the server computer since May, 2001. Most of the basic operations of the RARF are currently carried out without any serious problems.

We plan to apply the present EPICS control system for the RIBF accelerators as well. There is a demand that the system expansion should be carried out only by adding the parameters of new components into the EPICS database, if they are controlled by either the CAMAC or the GP-IB. It may be the easiest solution to expand the current system to the next one because the RIBF accelerators are similar to the RARF ones from the point view of control. However, both the interfaces have already become old and it is not a good idea to employ such old ones for the control of new components. Then it was decided to introduce three types of new control interfaces into the EPICS control system. The first one is NIO interface, which is used for new magnet power supplies. All magnet power supplies in the RIBF will be controlled by an NIO. In the RARF, we have already controlled the power supplies with the NIO in the extended beam line of the RILAC. The second one is a PLC, which is used for a new RF system and so on. The third one is an N-DIM, which is our original control device developed to substitute for the CAMAC-CIM/DIM system. In the RIBF control system, the N-DIM will be used for various purposes; to control all beam diagnostic equipments, all vacuum systems, driving systems for deflectors and so on. Furthermore, it is also planned to replace the CAMAC-CIM/DIM in the RARF with the N-DIM gradually. Table 3.6.1 shows the relation between the interface devices and the components of the RARF and the RIBF. Figure 3.6.1 shows a photograph of the N-DIM.

Table 3.6.1. Interface devices in the RARF/RIBF.

	RARF		
	RILAC	AVF/RRC	BT (existing)
Ion Source	Hard wire /WE 7000 (Yokogawa)	WE 7000 (Yokogawa)	
RF	PLC (Omron)	PLC (Sharp)	DIM
Magnet Power Supply	GP-IB/NIO/DIM	DIM	DIM/NIO
Beam Diagnostics	DIM/N-DIM	DIM	DIM
Driving Controller	DIM	DIM	DIM
Vacuum	N-DIM	PLC (Omron)	DIM
Beam Interlock	Hard wire /PLC (Mitsubishi)	DIM	DIM
Cooling	Local only	Local only	Local Only

	RIBF						
	fRC	BT (in Nishina)	BT (in new building)	IRC	SRC	Injection Line for Big-RIPS	Big-RIPS
Ion Source							
RF	PLC (Omron)	not fixed	not fixed	PLC (Omron)	PLC (Omron)		
Magnet Power Supply	DIM/NIO	NIO/DIM	NIO	NIO	NIO	NIO	NIO
Beam Diagnostics	N-DIM/DIM	N-DIM	N-DIM	N-DIM	N-DIM	N-DIM	not fixed
Driving Controller	N-DIM/DIM	N-DIM	N-DIM	PLC (Omron) /N-DIM	PLC (Mitsubishi) /N-DIM	not fixed	not fixed
Vacuum	Local only	N-DIM	N-DIM	PLC (Omron)	PLC (Mitsubishi)	N-DIM	not fixed
Beam Interlock	not fixed	not fixed	PLC (Mitsubishi)				
Cooling	Local only	Local only	PLC (Mitsubishi)				

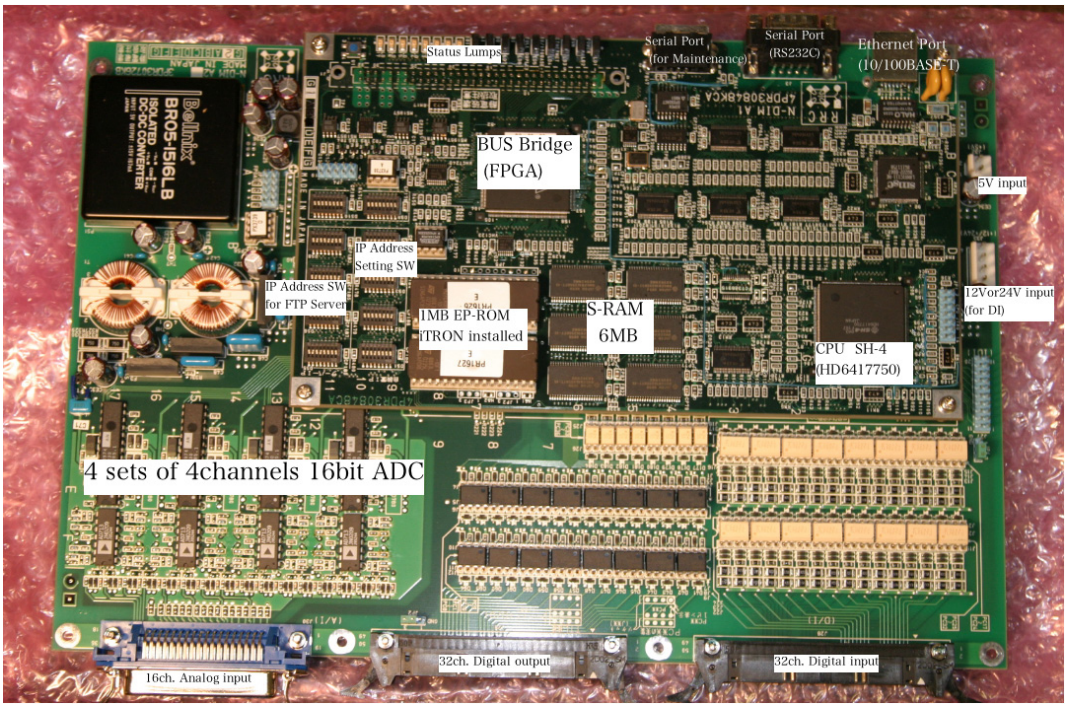

Figure 3. 6.1. Photograph of the N-DIM.

3.7 Design of the flattop resonator for the RRC

Since the beam-losses in the RRC might limit the final beam intensity, a study for energy-spread reduction by flattop acceleration is currently underway.

The flattop will be achieved by a third harmonic resonator with a frequency range of 54-120 MHz and a total peak gap voltage of roughly 135 kV. This new resonator could replace the valley box SE, which is currently used for phase-probes and three vacuum pumps. Its boundaries are limited by the location of the first and last turn, the injection and extraction bending magnets and the sector magnets E and S. Therefore, the available space is tight and it is challenging to find a resonator-shape that fits into the cyclotron.

In a first step, three different types of resonator geometries were investigated. The three-dimensional electromagnetic eigen-mode solver in ANSYS was used to simulate and compare a single-gap resonator with two double-gap resonators, one operated at the fundamental mode with phase-shift of 180° between the gaps and the other operated at a higher mode, doubled opening angle and phase-shift of 0°. For all three types, a geometry could be found that fits into the valley box. However, the fundamental-mode, double-gap resonator showed the most promising characteristics. It can be inserted into one half of the valley box, leaving the other half of the valley box free for the phase probes and the vacuum pumps. Furthermore, it requires less rf power than the other resonators and needs no intensive cooling on the liner location close to injection and extraction. However, the double-gap design has the disadvantage of reduced efficiency for some harmonic numbers, because of the fixed opening angle which can not have the optimal value for all cyclotron operation modes. Furthermore, the use of one half of the valley-box leads to small particle momentum kicks in radial direction, since one gap is necessarily not perfectly perpendicular to the trajectory of the particles.

The fully parameterized simulation model of one half of the resonator is convenient for the optimization of the resonator geometry. It was found that, at higher frequencies, a design with two stems is superior to a design with one stem only. Preliminary simulation results predicted a maximum quality factor of Q_0=13,900 at a frequency of 85 MHz and a minimum quality factor of Q_0=12,000 at 120 MHz. The highest current density in the shorting plate of 23 A/cm was found at a frequency of 113 MHz and the maximum electric field in the resonator of 3.7 MV/m at a frequency of 90 MHz. This is lower than half of Kilpatrick's electric field limit.

Figures 3.7.1 shows the shape of the resonator designed.

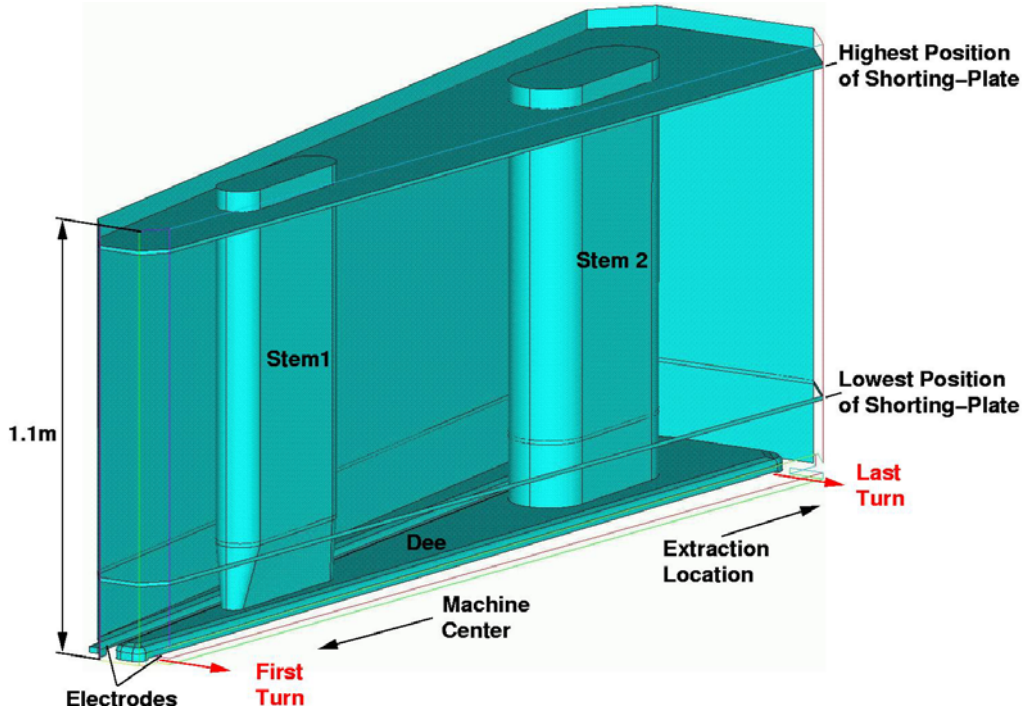

Figure 3.7.1. Layout of the proposed flattop resonator for the RRC. The upper half part of the resonator is shown. The vertical position of the shorting-plate is adjusted for the coarse tuning in the range of 54 MHz to 120 MHz. Facets on the outermost corners increase the space to the injection- and extraction magnets.

3.8 R&D on the production of U ion beam

The multi-charged U ion beams are planned to produce in the RIKEN 18 GHz ECR ion source from depleted UF_6 (predominantly ^{238}U). Although UF_6 is solid at room temperature, the vapor pressure (100 Torr at 20 deg.) is found to be adequate for use in the source without heating the sample. The beam intensity of U^{20+} (requested charge state) from the ion source is estimated to be 1~2 pμA at the extraction voltage of 10 kV (requested extraction voltage).

Generally speaking, to produce higher charge state heavy ions, such as U^{20+}, we need the gas mixing method. However, using UF_6, we may not need this method to obtain higher charge state of U ions, because the fluorine from the UF_6 will tend to force the U charge state distribution toward the higher values. The test experiment to produce U beam with this method is scheduled this November.